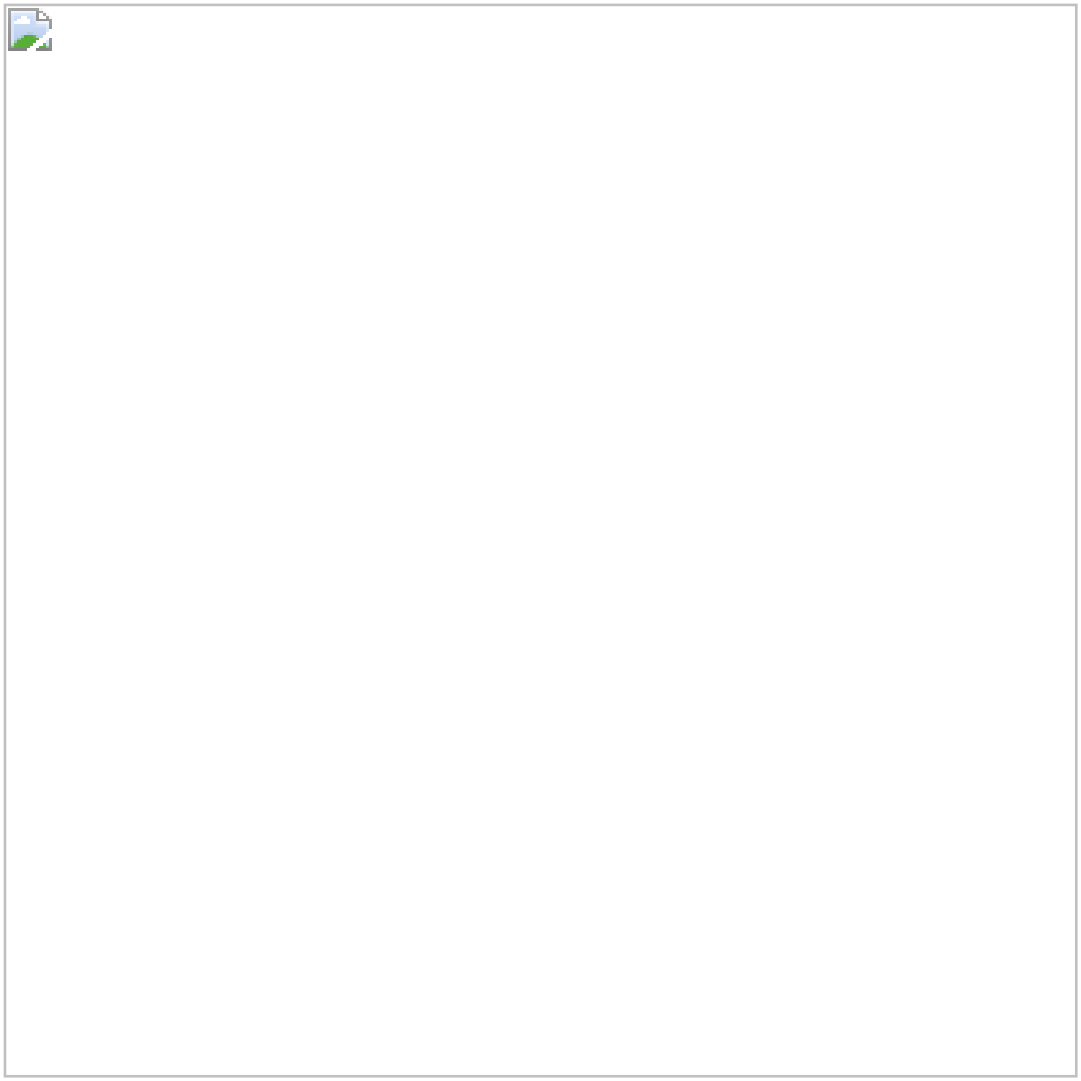

Thermal Erosion of a Permafrost Coastline: Improving Process-Based Models Using Time-Lapse Photography

Authors: Wobus, Cameron, Anderson, Robert, Overeem, Irina, Matell, Nora, Clow, Gary, et al.

Source: Arctic, Antarctic, and Alpine Research, 43(3) : 474-484

Published By: Institute of Arctic and Alpine Research (INSTAAR), University of Colorado

URL: https://doi.org/10.1657/1938-4246-43.3.474

Arctic, Antarctic, and Alpine Research, Vol. 43, No. 3, 2011, pp. 474–484

Thermal Erosion of a Permafrost Coastline: Improving Process-Based Models Using Time-Lapse Photography

*Cameron Wobus**†
Robert Anderson‡§
Irina Overeem‡
Nora Matell§
Gary Clow# *and*
Frank Urban#

*Cooperative Institute for Research in Environmental Sciences, University of Colorado, Boulder, Colorado 80309, U.S.A.
†Corresponding author. Present address: Stratus Consulting, Inc., 1881 Ninth Street, Boulder, Colorado 80302, U.S.A.
cameron.wobus@colorado.edu
‡Institute of Arctic and Alpine Research, University of Colorado, Boulder, Colorado 80309, U.S.A.
§Department of Geological Sciences, University of Colorado, Boulder, Colorado 80309, U.S.A.
#U.S. Geological Survey, Box 25046, Federal Center, Denver, Colorado 80225, U.S.A.

DOI: 10.1657/1938-4246-43.3.474

Abstract

Coastal erosion rates locally exceeding 30 m y^{-1} have been documented along Alaska's Beaufort Sea coastline, and a number of studies suggest that these erosion rates have accelerated as a result of climate change. However, a lack of direct observational evidence has limited our progress in quantifying the specific processes that connect climate change to coastal erosion rates in the Arctic. In particular, while longer ice-free periods are likely to lead to both warmer surface waters and longer fetch, the relative roles of thermal and mechanical (wave) erosion in driving coastal retreat have not been comprehensively quantified. We focus on a permafrost coastline in the northern National Petroleum Reserve–Alaska (NPR-A), where coastal erosion rates have averaged 10–15 m y^{-1} over two years of direct monitoring. We take advantage of these extraordinary rates of coastal erosion to observe and quantify coastal erosion directly via time-lapse photography in combination with meteorological observations. Our observations indicate that the erosion of these bluffs is largely thermally driven, but that surface winds play a crucial role in exposing the frozen bluffs to the radiatively warmed seawater that drives melting of interstitial ice. To first order, erosion in this setting can be modeled using formulations developed to describe iceberg deterioration in the open ocean. These simple models provide a conceptual framework for evaluating how climate-induced changes in thermal and wave energy might influence future erosion rates in this setting.

Introduction

The impact of climate change on landscape evolution may be more pronounced in the Arctic than in other landscapes, due to the direct influence of temperature on geomorphic processes in this setting. The physical processes that drive landscape evolution in most settings are supplemented in these areas by thermal processes, whereby the thawing of ice-rich soils can lead to rapid and dramatic changes in landscape form. Arctic coastlines are especially susceptible to changes in climate, since warming of the landscape along the coast is accompanied by significant changes in offshore sea ice conditions (e.g., Serreze et al., 2007). These changes in the offshore environment may influence factors such as sea surface temperatures (SST), wave energy, and the atmospheric conditions that generate storms during the open water season. Combined, these changes along the arctic land-sea interface generate conditions that might be expected to accelerate coastal erosion.

Against this backdrop, coastal erosion rates of ~20 m y^{-1} have been documented along segments of the Beaufort Sea coast (Harper, 1990; Solomon, 2005; Jones et al., 2008), and two recent remote sensing studies suggest that coastal erosion rates have been increasing along parts of this coastline over the past few decades (e.g., Mars and Houseknecht, 2007; Jones et al., 2009). Both of these latter studies suggested that some combination of warming waters and increasing wave energy has been responsible for the apparent acceleration in coastal erosion rates. What previous studies have thus far been lacking, however, is a time series of direct observational evidence that allows a process-based understanding of how this coastline evolves.

Our approach has been to combine measurements of coastal bluff substrate properties with direct observations of erosion processes and meteorological conditions to improve our process-based understanding of coastal erosion in this landscape (Kobayashi, 1985; Aré, 1988; Kobayashi et al., 1999; Hoque and Pollard, 2009). We collected time-lapse photography to monitor coastal erosion rates, collected samples of permafrost bluffs for laboratory analysis, installed benchmarks to document seasonal changes in coastline position, and measured eroded block and ice-wedge polygon dimensions. Our observations, coupled with direct and remotely sensed observations of meteorological conditions, sea ice conditions, water surface elevation, and sea surface temperatures, allow us to observe and quantify the drivers of coastal erosion in this setting. Our data indicate that the undermining of permafrost bluffs by melting of interstitial ice is the rate-limiting process driving coastal erosion in this setting, much as thermal notching at the waterline drives the deterioration and calving of icebergs (e.g., Russell-Head, 1980; White et al., 1980; Kubat et al., 2007). To first order, modeling frameworks initially developed for quantifying rates of iceberg deterioration are therefore used as a conceptual backdrop for understanding rates of erosion in this setting. Although more complex models describing a broader suite of physical processes have been described in detail (e.g., Kobayashi, 1985; Kobayashi et al.,

1523-0430/11 $7.00

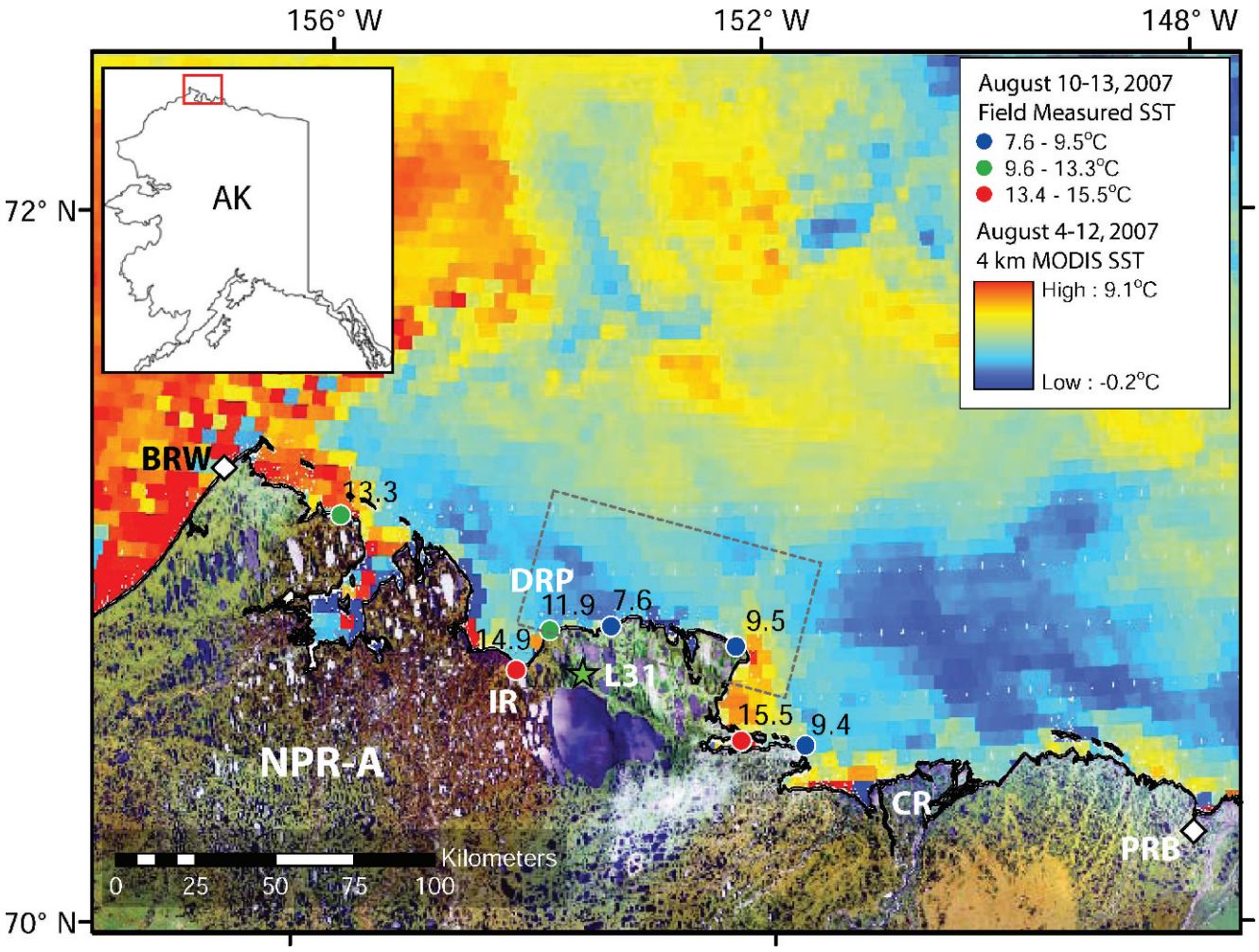

FIGURE 1. Site location map, with MODIS-derived SST from early August 2007 and point measurements of SST collected during August 2007. Thin dashed box shows the region from which time series of SST was calculated for the comparison shown in Figure 8. BRW = Barrow; PRB = Prudhoe Bay; CR = Colville River; IR = Ikpikpuk River; DRP = Drew Point; L31 = Lake 31. Inset shows location of field site in northern Alaska.

1999), we propose that our simple description of bluff erosion as a dominantly thermal process captures the first-order behavior of how this coastline evolves. Furthermore, this simplified framework provides a direct and attainable route to assessing the role of climate change on coastal erosion in the Arctic. Further work is ongoing to improve our empirical model of surface setup and to understand the drivers of ocean heat transport in this setting.

Study Site

Our investigation focuses on the Beaufort Sea coast approximately halfway between Barrow and Prudhoe Bay, within

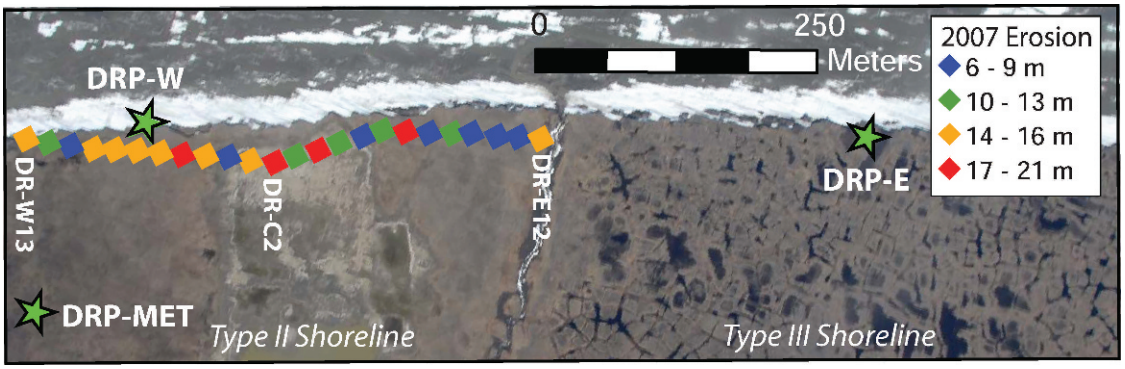

FIGURE 2. IKONOS image of Drew Point coastline with locations of time-lapse photography and meteorological stations. Colored diamonds show total erosion measured in the field between 8 August 2007 and freeze-up in late September (2007 data are shown to illustrate variability along full section of monitored coastline; see Fig. 9 for comparison between 2007 and 2008 measurements). Base image courtesy of B. Jones, U.S. Geological Survey.

FIGURE 3. Selected images from timelapse sequences at (A) DRP-W and (B) DRP-E cameras. Middle image in DRP-W images shows position of measurement points for quantitative estimates of melt rates shown in Figure 6. DRP-E sequence shows rapid thermal disintegration of ~2-m-wide calved block once it falls into the sea.

the National Petroleum Reserve–Alaska (NPR-A; Fig. 1). This portion of the Beaufort Sea coastline is characterized by a low-relief coastal plain in which most of the topography is related to shallow depressions (tens of centimeters to a few meters deep) formed by 1- to 10-km-diameter thaw-lake basins. Coastal bluffs along the shoreline are typically 2–5 m high and represent the only other significant topographic relief within the study area. Bathymetric gradients are also low: the 10 m isobath is >10 km offshore (Greenberg et al., 1981), and narrow beaches are exposed along much of the coastline only when offshore winds depress water levels in the sea. This ice-rich bluff morphology is representative of much of the NPR-A coastline, as well as other segments of the Alaskan and Canadian Beaufort Sea coastlines (Harper, 1990; Jorgenson and Brown, 2005).

Surficial deposits primarily comprise Quaternary marine silt and clay, punctuated in the western portion of the study area by Quaternary alluvial plain and terrace deposits and throughout the region by mudflats recording the positions of breached thaw-lake basins (Williams et al., 1977; Carter and Galloway, 2005). The Colville River is the main regional source of clastic material to the Beaufort Sea, supplemented locally by smaller rivers including the Ikpikpuk and sparse coarse-grained deposits within eroding coastal bluffs (Reimnitz et al., 1988; Rachold et al., 2000; Jorgenson and Brown, 2005). The entire region is underlain by continuous permafrost to depths of 200–400 m, with an active layer—the surface zone subjected to annual thawing during the warmest summer months—typically ~0.3–0.5 m thick (Clow, 1998). Most of the landscape is covered by peat and grass whose roots form a cohesive blanket that closely coincides with the active layer.

Recent studies have documented coastal erosion rates as high as 20 m y^{-1} along segments of the Beaufort Sea coastline using remote sensing and repeat mapping of coastal position (Reimnitz et al., 1985; Jorgenson and Brown, 2005; Mars and Houseknecht, 2007; Jones et al., 2008, 2009). Since all of this erosion must occur during the short ice-free season, these documented rates indicate that summertime erosion is rapid enough to be directly observable using time-lapse photography.

Methods

We deployed two time-lapse cameras along the Beaufort Sea coast, near Drew Point, to observe coastal retreat during the summer of 2008 (Figs. 1 and 2). Photographs at the two sites (DRP-W and DRP-E) were collected every 2 h between 20 June and 2 August. Quantitative records of coastal erosion rates were constructed from time-lapse imagery for each site. Distances from a fixed reference point to the shoreline were measured from imagery at time intervals ranging from 4 h to 12 h and calibrated using an image from each time-lapse sequence in which a 2-m-high stadia rod was captured. Quantitative estimates of bluff retreat are limited to the period between 20 June and 28 July since a severe windstorm at the very end of the record fogged the camera lens, making the record difficult to interpret quantitatively. Cameras were retrieved just before collapse of the bluffs onto which they were anchored (timelapse movie is available: <http://csdms.colorado.edu/wiki/Movie:ArcticErosion>).

At site DRP-W measurements were made at three points along the bluff: the top of the vegetative mat; the middle of the bluff face; and the base of the bluff near the waterline (Fig. 3, a). At site DRP-E, the vantage point did not allow direct observation of the bluff face, but the disappearance of an eroded block from the water provides a view of the rapid degradation of an eroded block in the shallow sea (Fig. 3, b). We estimate that our direct observations of bluff face position along the Beaufort Sea coast are accurate to within approximately 5–10 cm.

Our field observations were designed to characterize the material making up the coastal bluffs, the size distribution of

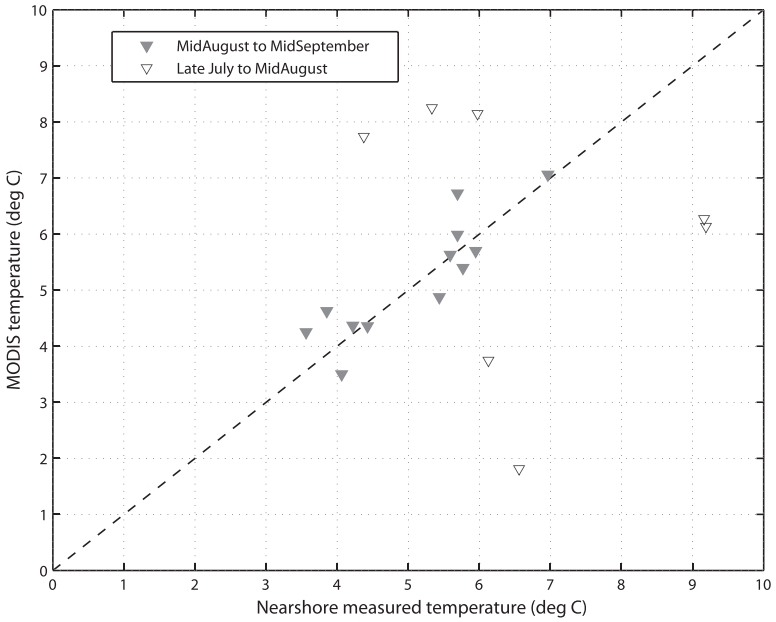

FIGURE 4. Comparison of nearshore measured SST and MODIS estimated SST based on maximum temperature within the box shown in Figure 1. Line through origin has a slope of 1 and an R^2 value of 0.75.

eroded blocks, and the location of weakness planes along the coastline. Sixteen bulk samples were chipped from the frozen bluffs and collected for laboratory analysis. Bulk samples were weighed in the laboratory to characterize total mass, which ranged from 0.2 to 1.4 kg. Samples were then dried and re-weighed to determine total ice content by mass. A subset of these samples was then analyzed for total organic content via loss on ignition. The dimensions of eroded blocks and of ice-wedge polygons along upland surfaces were measured by field survey.

As described below, our field and time-lapse camera observations support a simplified mechanism of coastal erosion whereby thermally driven notching at the toe of the bluffs drives block collapse and failure. Modeling of this thermal notching process requires data describing sea surface temperature, wave climate, and the wind conditions under which the water surface is pushed against the bluff face. Our modeling is informed by a combination of field and remotely sensed measurements of ocean and meteorological conditions.

Sea surface temperatures were intended to be measured using autonomous temperature sensors deployed immediately offshore and anchored to the shoreline. Unfortunately, these sensors were lost when the bluffs onto which they were anchored were undermined and collapsed. As a result, water temperature records from the Beaufort Sea sites were compiled from remotely sensed records of sea surface temperatures, using the 8-day binned Level III SMI MODIS product (Walton et al., 1998). Raw data is available from http://oceancolor.gsfc.nasa.gov/. Sea surface temperatures near Drew Point were estimated from these 8-day binned data by compiling minimum, maximum, and mean SST within an approximately 50 km × 80 km box directly offshore (Fig. 1). This MODIS SST product is gridded at 4 km resolution; the 50 km × 80 km size of the MODIS box was chosen to provide a local estimate of SST while minimizing the effects of potential outliers.

Although the loss of our instrumentation made it impossible to evaluate the correlation between the MODIS-averaged and nearshore SST during 2008, an offshore buoy we installed during the summer of 2009 provides an approximately 2-month overlap with the MODIS record from that year. The data from most of that monitoring period indicate a good correlation between measured and MODIS-estimated SST (R^2 = 0.76 for a slope of approximately 1; see Fig. 4). A smoothed curve was fit to the 8-day maximum data as a model input for the daily sea surface temperature. A better understanding of the thermal structure of the nearshore environment is beyond the scope of this paper; however, for purposes of our model evaluation, we rely on this distillation of remotely-sensed SST to drive the temperature component of our model.

Wave heights over the time-lapse monitoring period were modeled using a fetch-limited, shallow water wave model (U.S. Army Corps of Engineers, 1984). Wind speed and direction were compiled from a meteorological station at Drew Point (Fig. 1), and fetch was determined from the distance to the sea ice edge in the upwind direction. Superimposed on this wave model is a simplified parameterization of surface setup in which the wind direction is the primary control on when the water surface is in contact with the bluff face (Wobus et al., 2010). Details of the wave model are provided in Overeem et al. (in review).

Results

SUMMARY OF TIME-LAPSE PHOTOGRAPHY OBSERVATIONS

Our time-lapse imagery allows us to place coastal erosion into the broader context of offshore conditions, such as the concentration of sea ice immediately offshore, the size of incoming waves, and changes in water levels due to surface winds (setup). General observations from our time-lapse photography installations are as follows:

- Erosion prior to the disappearance of sea ice is accomplished by slow, subaerial melting along the entire bluff face.
- After the disappearance of floating sea ice, erosion accelerates near the waterline and vastly outpaces subaerial melting along the remainder of the bluff.
- Once sea ice disappears, erosion rates at the waterline vary markedly with time, giving a stepped appearance to a plot of cumulative erosion.
- Once frozen blocks are undermined and detach from the bluff face, they deteriorate very rapidly in seawater.

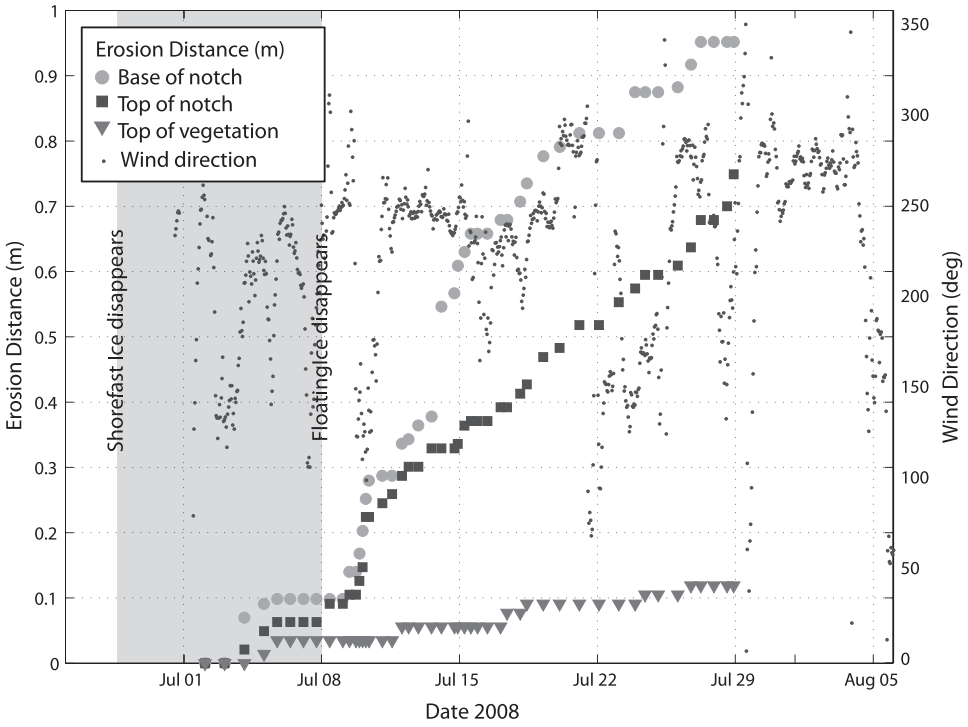

FIGURE 5. Measured bluff retreat at DRP-W camera site based on time-lapse imagery. Bluff positions from bottom to top, as shown in Figure 3, A, are shown as circles, squares, and diamonds, respectively, as measured on left *y*-axis. Small blue dots show wind direction, as measured at station DRP-MET (see Fig. 2) and shown on right *y*-axis. Note rapid increase in retreat rate after last appearance of floating sea ice.

DRP-E TIME-LAPSE SEQUENCE

The vantage point at site DRP-E did not allow direct observation of erosion at the waterline. However, this time-lapse sequence provides a view of the fate of an eroded block once it has fallen into the sea. Failure of an ~2-m-long block at this site occurs on 21 July, once the undermining at the base of the bluff is sufficient to destabilize it. Degradation of this eroded block occurs rapidly once it has fallen into the shallow sea, and the block has completely disappeared by 28 July (see Fig. 3, b). Furthermore, these images indicate that block failures do not create any strong negative feedbacks on erosion rates in this setting for two reasons: first, the nature of the block failure is such that seawater has access to the bluff face within one day of the block collapse (Fig. 3, b). The images we have collected therefore indicate that collapsed blocks may not create a buffer between the frozen bluffs and the sea. Second, owing to the high ice content of these permafrost bluffs, there is no remnant of this block left behind once its thermal degradation is complete. These observations of the fate of an eroded block after failure support the hypothesis that detachment of the blocks, rather than their degradation, is the rate-limiting process driving erosion along this segment of the NPR-A coastline.

DRP-W SITE TIME-LAPSE SEQUENCE

The camera at site DRP-W provided the best vantage point to observe the process of bluff retreat. This sequence was therefore used to quantify the progression of notch formation through time. Prior to the disappearance of sea ice from the imagery, bluff position remains relatively stable, with total erosion between 28 June and 8 July limited to approximately 10 cm (Fig. 5). Field observations indicate that the major process driving coastal change prior to the disappearance of sea ice is slow subaerial melting of the exposed permafrost on the bluff face and flow of the resulting unconsolidated mud under gravity. Using daily measurements from wooden dowels as erosion pins, the rates of this thermal degradation were measured at ~1 to 6 cm day^{-1} during late June, when air temperatures ranged from ~0.5 to 10 °C. Based on our observations, rates of this subaerial thermal degradation do not appear to be aspect-dependent: thermal degradation rates on north- and northwest-facing bluff faces were equal to or greater than those along south-facing blocks. As suggested by Aré (1988), this lack of aspect dependence is likely due to a combination of the diffuse sunlight in the Arctic and the relatively even exposures to sunlight from all directions during the polar day.

Although subaerial thermal degradation clearly contributes to the overall retreat of the coastline, this process becomes subsidiary to the undermining of the bluff at the waterline after the disappearance of floating sea ice on 8 July. Both the overall rate of bluff retreat and the divergence between the base and top of the bluff accelerate after the last appearance of floating sea ice on 8 July (Fig. 5). Erosion after 8 July is focused along a notch near the waterline where the rate of bluff retreat outpaces the rate above the top of the notch by as much as a factor of two. Throughout the monitoring period, retreat of the top of the bluff is negligible due to the strength of the vegetative mat at the surface.

Maximum wind speeds over this recording interval were approximately 7 m s^{-1}, and maximum wave heights observed in our time-lapse photography sequence were <0.5 m. The progression of notch erosion over this interval (approximately 1 m in 3 weeks) indicates that erosion can proceed even in relatively quiet seas. This notch formation is consistent with the "thermal abrasion" process described by Aré (1988), in which erosion is driven by the efficient delivery of heat to the bluff face via the mechanical mixing of nearshore waters. Progression of erosion in the absence of significant storm activity indicates that relatively little mechanical energy is required to accomplish this mixing. In this sense, the term *thermal abrasion* is in fact misleading, as abrasion implies a direct role for mechanical energy.

Although our observations indicate that erosion proceeds even in the absence of significant storm-driven waves, setup of the water surface by wind is required for seawater to access the bluff face. As illustrated in our time-lapse photographs, the bluff face is

FIGURE 6. Example of the magnitude of surface setup and setdown driven by wind events at Drew Point. Winds are ~4 m s^{-1} from the NE in the top photo, and ~4 m s^{-1} from the E in the bottom photo.

sheltered from seawater much of the time by a narrow shelf (Fig. 6). This shelf is most commonly lost when winds are from the north, during which time relatively warm seawater can access the bluff face and erosion can proceed. These surface setup events can be on the order of 0.5–1 m, in a setting where the normal tidal range is on the order of only 0.15 m (e.g., Reimnitz and Maurer, 1979). Setup events therefore create an environment in which periods of thermal erosion are punctuated by periods in which erosion slows dramatically because the bluffs are not in contact with seawater at all. The erosion rate therefore appears ''stepped'' through time, as shown in Figure 5.

Other Field Observations and Measurements

Observations along the base of the bluffs during the summer of 2008 demonstrate that block failures are commonly controlled by planes of weakness associated with ice wedges. We measured eroded block dimensions along an approximately 4.5 km stretch of the shoreline. We also measured the dimensions of 111 high-centered frost polygons just onshore from our eastern camera installation (Fig. 1). Histograms of these two size distributions are very similar, with the expected shift in the size distribution of eroded blocks due to degradation once block failure has occurred (Fig. 7). In many cases, remnants of ice wedges were still present along recently exposed bluff faces, giving the appearance from the sea that the stratigraphy included lenses of massive ground ice. These sites in which block failures were clearly ice-wedge controlled were present in approximately 40% of the sites where eroded blocks were observed. While clear evidence of ice wedge control was absent from the other blocks, our observations indicate that ice wedges represent planes of failure approximately half the time, and possibly much more (Hoque and Pollard, 2009).

Collection and analysis of bluff samples indicates that intact bluffs are resistant to physical impacts and abrasion, but have relatively limited resistance to warming. Samples for laboratory analysis were collected using ice picks and shovels, and required repeated blows with both instruments to dislodge even small flakes from the frozen bluffs. Analyses of the 16 composite bluff samples indicate that frozen bluffs along this portion of the NPR-A coastline comprise between 50 and 80% ice by mass (Table 1). The remainder of the bluff material is dominated by organics (~10–30%) and silt and clay-sized mineral matter. Melting of interstitial

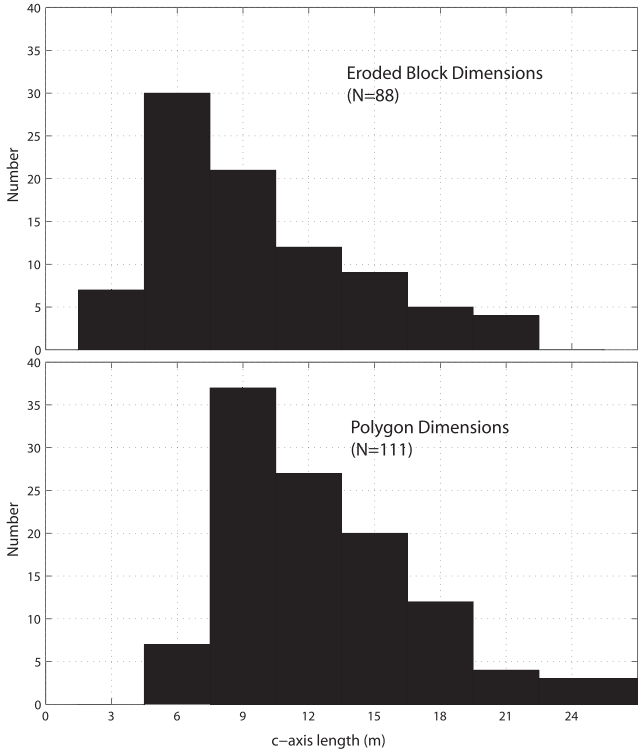

FIGURE 7. Histograms of (A) eroded block dimensions, and (B) frost wedge polygon dimensions from field surveys conducted during the summer of 2008.

ice therefore creates a fine-grained, organic-rich residue representing less than 50% of the volume of intact bluffs, all of which can be easily transported away from the coastline in suspension.

Summary of Observations

Combined, our observations indicate that the undermining and block failure of the bluffs, rather than degradation and transport of eroded block material, controls the rates of coastal erosion in this environment. Furthermore, the progression of erosion during relatively quiet seas and the significant mechanical strength of the bluff materials indicate that thermal, rather than mechanical, processes will control the notching and destabilization of coastal bluffs in this setting. To first order, we therefore hypothesize that coastal erosion can be approximated as a thermal process: melting of interstitial ice, rather than mechanical abrasion or transport of eroded material, should be rate-limiting. A caveat to this conceptual model is that surface winds must have a northerly component in order to push seawater into contact with the bluff face (see Fig. 6); during southerly winds, a shelf develops between the bluffs and the sea that insulates the coast from erosion.

Model Evaluation

We describe thermal erosion of the notch using simple models developed to describe iceberg deterioration in open water (e.g., Russell-Head, 1980; e.g., White et al., 1980; Kubat et al., 2007). Sea surface temperatures were derived from a smoothed fit to the 8-day binned Level III SMI MODIS product, as described above (Walton et al., 1998). Setup events are parameterized as periods where winds have a northerly component. Based on our time-lapse observational record, setup events also occur during west-southwest winds, so we also include winds from the west-southwest (i.e., between 250° and 270°) in our setup-inducing wind events. We use daily average wind direction from the Drew Point meteorological station (DRP-MET on Fig. 2) to parameterize this surface setup.

We recognize that a number of models that explicitly account for mechanical mixing, convective heat transfer, and other processes have been proposed to describe the thermoabrasion process (e.g., Kobayashi, 1985; Kobayashi et al., 1999; e.g., Costard et al., 2003). However, we excluded these models from our final analysis for three reasons. First, the open Beaufort Sea exposes the coastline to sufficient incoming wave energy that offshore waters are well mixed (i.e., turbulent heat transfer is not likely to be rate limiting). Second, sensitivity analyses conducted by Kobayashi et al. (1999) indicate that temperature is far more important than mechanical properties of the substrate in controlling erosion rates[1]. Finally, due to the difficulties associated with primary data collection in this setting, we lack the supporting information to quantify all of the variables that a model of this sort requires. Calibrating our observations to these more complex models would therefore place us in a position of having a substantially under-constrained problem. While the models described below are meant to be first order, they improve our ability to evaluate the sensitivity of coastlines in this setting to potential future changes in climate.

POWER-LAW MODEL

A number of experimental studies have shown that the melt rate of icebergs in seawater can be expressed as a simple power function of the water temperature (c.f., Holland et al., 2008). Generically, the melt rate can be expressed as:

$$M = \alpha(T_s - \delta)^{\beta} \tag{1}$$

where M is the melt rate in cm s^{-1}, T_s is the temperature of the water bath in °C, α and β are empirically derived constants, and δ is the freezing point of the water bath. Experimental results indicate that the exponent β is generally between 1 and 2 (e.g., Griesman, 1979; Russell-Head, 1980; e.g., Josberger and Martin, 1981).

In calculating the thermal erosion potential from the power-law model, we adopt the empirical constants derived by the experimental work of Russell-Head (1980), where $\alpha = 2.08 \times 10^{-7}$, $\beta = 1.5$, and $\delta = -1.8$ °C (the approximate freezing temperature of seawater with salinity of 35‰, which is close to the few values we were able to measure in the field). Note that the freezing point is lower than 0 °C even for freshwater ice, due to the mixing of saline waters along the ice interface (e.g., Russell-Head, 1980). Using the maximum 8-day MODIS SST as a proxy for nearshore temperature, this model tracks the observed time series of coastal erosion quite well over the course of our short monitoring period (Fig. 8). Over the entire summer 2008 open-water season, the model predicts a total of 10.7 m of erosion. An additional 4.1 m of erosion occurred between ice breakup and the end of July 2009 when the distance from benchmarks to the coast

[1] In Kobayashi et al. (1999) a 4.5 °C change in the sea surface temperature leads to a quadrupling of total notch erosion over a 2-day modeling period, whereas completely removing all coarse sediment (equivalent to decreasing the resistance to mechanical erosion) leads to a change in notch erosion rate of only 25% (Kobayashi et al., 1999). Based on these sensitivity analyses, notch erosion in the Kobayashi model is therefore driven to first order by thermal energy.

TABLE 1

Bulk properties of permafrost bluffs from Drew Point.

Sample ID	Frozen mass (g)	Dry mass (g)	Ice mass (g)	Ice content (wt %)
08LB1	429.55	22.18	407.37	94.8
L31-Bluff	1002.05	206.15	795.9	79.4
08P-RC1	288.67	80.64	208.03	72.1
08P-RC2	527.45	279.56	247.89	47.0
08L-RC3	325.77	141.28	184.49	56.6
08L-RC4	90.23	28.36	61.87	68.6
08L-RC5	533.25	312.64	220.61	41.4
08L-RC6	209.55	68.56	140.99	67.3
08P-Bulk1-MP	722.07	266.94	455.13	63.0
08P-Bulk1-IFSB	1307.23	691.55	615.68	47.1
08P-Bulk2-DBP	986.94	182.86	804.08	81.5
08P-Bulk2-LBSS	1388.12	766.4	621.72	44.8
08L-Strat01-DBCS	1147.36	392.2	755.16	65.8
08L-Strat01-IFSB	862.55	378.85	483.7	56.1
08L-Bulk02-MGM	970.59	182.92	787.67	81.2
08L-Bulk02-DBCS	712.4	272.54	439.86	61.7
			Average Ice Content	64.3

were re-measured. Thus the total coastal erosion predicted by this model between our 2008 and 2009 field seasons is approximately 15 m. For comparison, the average of our measurements of coastal retreat between mid-June 2008 and late July 2009 was ~15.5 m (Fig. 10).

THERMAL-WAVE MODEL

We evaluated a second set of models that explicitly considers wave height, wave period, and roughness length scale in forming an erosional notch at the waterline. As described by White et al. (1980), the erosion rate along a rough-wall surface is independent of the flow Reynolds number, but can be shown to be related to the roughness height as a fraction of the wave height (R/H) and to the wave period τ, in addition to the temperature difference between water and ice, ΔT:

$$V_{we} = 0.000146\left(\frac{R}{H}\right)^{0.2}\left(\frac{H}{\tau}\right)\Delta T$$

where V_{we} is the melt rate in m s^{-1}. Note that while wave height is explicitly considered in this formulation, temperature exerts more leverage on erosion rates than does wave height, both because the exponent on ΔT is larger (1 vs. 0.8) and because there is an effective upper bound on wave height in shallow seas that does not exist for sea surface temperatures. We assume an ice temperature of 0 °C for these calculations.

Wave heights were calculated for the summer open-water season using a fetch-limited shallow water wave equation, driven by the observed meteorological conditions at Drew Point and a sea ice edge position derived from remotely sensed observational data (U.S. Army Corps of Engineers, 1984; Overeem et al., in review). As with the power-law model, it was also assumed that thermal erosion by seawater progresses only when the wind direction has a northerly component that can push seawater over the exposed beach and against the bluff face. Based on our observational data, we assumed a roughness length scale of 1.0 cm, and a wave period of 10 s for these calculations.

As shown in Figure 8, the thermal-wave model predicts a slightly greater magnitude of erosion than the power-law model for the same period of monitoring. Over the summer of 2008, the thermal-wave model predicts approximately 15 m of erosion, compared to approximately 11 m of erosion for the power-law model. As with the power-law model, the progression of erosion using the thermal-wave model is also sensitive to the daily average wind direction, which in our formulation determines whether erosion proceeds or stalls on any given day.

Summary of Erosion Models

The overall magnitude of erosion predicted by both models is in relatively good agreement with average observed erosion rates of ~15 m y^{-1} along this coastline (Fig. 9). Our observations of surface setup and setdown also provide a straightforward explanation for the stepped appearance of erosion rates through time: periods in which thermal erosion can proceed are punctuated by periods in which the bluffs are insulated from seawater by an exposed bench. These observations suggest that a primarily thermal mechanism of erosion is a reasonable explanation for observed rapid coastal loss along the NPR-A coastline.

Both of the erosion models evaluated here are primarily thermally driven. Sensitivity analysis indicates that an increase in the average temperature of just 1 °C increases erosion rates in both models by approximately 30%. An increase in average wave height of 10% increases erosion rates in the thermal-wave model by ~10%. As described below, the major controlling variable that is not yet well constrained is the surface setup.

Evaluation of the two erosion models indicates that the daily thermal erosion potential ranges from less than 0.5 to more than 1.5 m day^{-1}, depending on whether a power-law or thermal-wave model is chosen (Fig. 10). Given these high erosion potentials, the major controlling variable in either model is therefore the number of days during the open-water season that surface setup is sufficient to expose the bluff toe to these thermally erosive waters. Our model assumes a simple relationship between wind direction and surface setup, which is based on observational data from time-lapse photography during the summers of 2008 and 2009. However, given the leverage that this parameter exerts on the total erosion realized during the year, a more rigorous treatment of the meteorological parameters driving surface setup is required.

Discussion and Conclusions

We have used field measurements and observations, sea surface temperature data, and time-lapse photography from permafrost bluffs in the NPR-A to better understand the mechanisms driving extremely rapid coastal erosion along permafrost bluffs. Our observations indicate that (1) notch formation, rather than block disintegration, is rate limiting in this setting; (2) the high ice content and high mechanical strength of these permafrost bluffs make them very susceptible to thermal erosion but relatively resistant to mechanical erosion; and (3) wind direction plays a major role in controlling notch formation, by controlling how frequently seawater has access to the base of the bluffs.

Late summer storms have been observed to create substantial coastal loss in the Arctic over very short time scales. We hypothesize that the role of these storms in driving retreat of permafrost bluffs such as those in the NPR-A is primarily via their influence on thermal processes. First, surface setup by wind stress pushes saline seawater over the narrow beach, allowing thermal notching to progress at the base of the bluffs. Many of the strongest late-summer winds are from the north and northeast, which would be most effective in creating surface setup along the

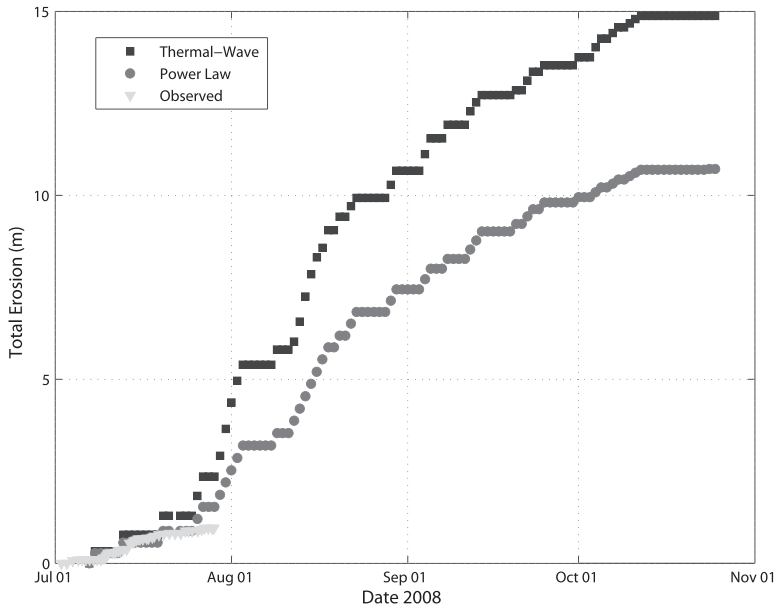

FIGURE 8. Measured erosion from time-lapse sequence at DRP-W superimposed on power-law and thermal-wave modeled erosion for the summer of 2008.

shore. Larger late-season storms that create longer and more significant periods of surface setup therefore play a crucial role in the overall development of this coastline through their modulation of thermal erosion processes. Documented storm surges of greater than 3 m (e.g., Reimnitz and Maurer, 1979; Harper et al., 1988) could drive thermal erosion along virtually the entire bluff face, which helps to explain anecdotal observations of accelerated coastal erosion during these events (e.g., Kobayashi et al., 1999).

Second, storm energy must play a role in coastal erosion by improving the efficiency of ocean mixing. Field measurements of sea surface temperature in August 2007 (Fig. 1) indicate that the shallow shelf offshore from Drew Point can hold large stores of warm water during the summer, which when effectively circulated along the bluff face by wave action will enhance thermal notching. To the extent that stores of warm water are available offshore, late summer storms could help to transport this heat shoreward.

Third, although these permafrost bluffs along the NPR-A coastline have a high ice content, their erosion must create a lag of fine-grained deposits, some of which is likely to be deposited close to the shore. Over the long term, the lateral retreat of the coastline must be accompanied by lowering of the subsea permafrost in order to continue (e.g., Aré, 1988). Removal of this "thermal blanket" from the sea floor may therefore be an important process in allowing shoreline retreat to be maintained on longer time scales. Thus the mechanical role of waves may be more important in dealing with the materials immediately offshore than in driving erosion along the bluff face itself.

Climate change in the Arctic is resulting in ever-decreasing sea ice minima, longer open water seasons, and increasing distances to the sea ice edge in mid- to late summer (e.g., Serreze et al., 2007; Overeem et al., in review). These combined effects will increase both the total heat stored in the ocean and the total

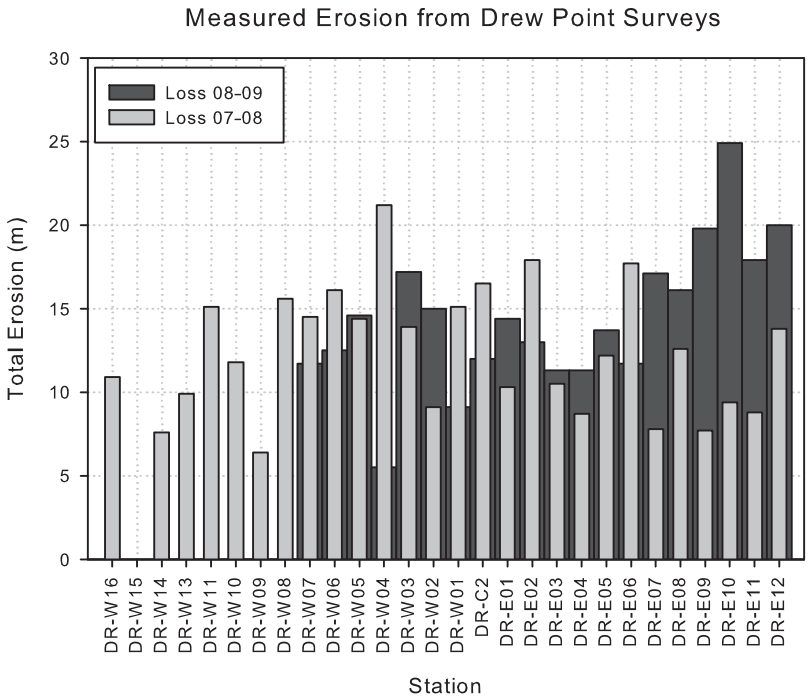

FIGURE 9. Measured erosion from benchmarks along Drew Point coastline between two monitoring periods: August 2007 to June 2008 (light gray bars) and June 2008 to July 2009 (dark gray bars). Benchmark locations are shown in Figure 2.

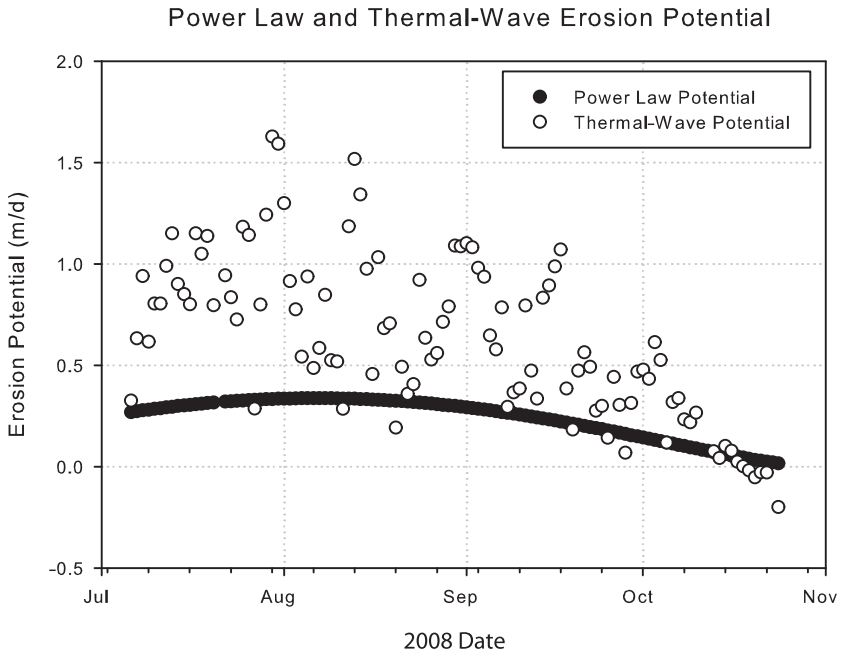

FIGURE 10. Total daily erosion potential for power-law and thermal-wave models, assuming seawater is in contact with bluff toe at all times. Note that the total seasonally integrated erosion dramatically exceeds observations, underscoring the importance of surface setup in controlling realized erosion.

integrated wave height over the summer season, both of which will play a role in accelerating coastal erosion with future climate change (e.g., Mars and Houseknecht, 2007; Jones et al., 2009). Our time-lapse photography, coupled with field and laboratory measurements, demonstrate that coastal erosion in this setting is primarily thermally driven. A warming Arctic will therefore have a direct and tangible influence on coastal erosion rates. However, based on the leverage that sea surface setup events exert on seasonally integrated coastal erosion, prediction of future changes in erosion rates will require a better understanding of the particular wind conditions driving surface setup events, and the expected changes in synoptic weather patterns associated with a warming Arctic.

Acknowledgments

This research was supported by the Office of Naval Research through the National Oceanographic Partnership Program (NOPP) under grant number 1543943. This work reflects close cooperation between the U.S. Geological Survey (USGS) and academic researchers (University of Colorado at Boulder; Naval Postgraduate School). We acknowledge logistical support from CH2MHill Polar Services, from the U.S. Bureau of Land Management, and from Ben Jones at USGS in Alaska. We thank Robert Brower and Eben Brower, our faithful bear guards, for their companionship and sharing of local knowledge of the Drew Point coastline. We thank Glenn Dunmire of Siku Construction for his assistance during our fieldwork in 2009. We also thank our reviewers for suggestions that improved this paper.

References Cited

Aré, F. E., 1988: Thermal abrasion of sea coasts. *Polar Geography and Geology*, 12: 1–157.

Carter, L. D., and Galloway, J. P., 2005: Engineering geologic map of the Harrison Bay quadrangle, Alaska. *U.S. Geological Survey Open-file Report 2005-1194*: scale 1:250,000.

Clow, G. D., 1998. Borehole locations and permafrost depths, Alaska, USA: Boulder, Colorado: University of Colorado, National Snow and Ice Data Center.

Costard, F., Dupeyrat, L., Gautier, E., and Carey-Gailhardis, E., 2003: Fluvial thermal erosion investigations along a rapidly eroding river bank: application to the Lena River (central Siberia). *Earth Surface Processes and Landforms*, 28: 1349–1359.

Greenberg, J., Hart, P. E., and Grantz, A., 1981: Bathymetric map of the continental shelf, slope and rise of the Beaufort Sea north of Alaska. *U.S. Geological Survey Miscellaneous Investigation Series Map I-1182-A*, scale 1:500,000.

Griesman, P., 1979: On upwelling driven by the melt of ice shelves and tidewater glaciers. *Deep Sea Research*, 26: 1051–1065.

Harper, J. R., 1990: Morphology of the Canadian Beaufort Sea coast. *Marine Geology*, 91: 75–91.

Harper, J. R., Henry, R. F., and Stewart, G. G., 1988: Maximum storm surge elevations in the Tuktoyaktuk region of the Canadian Beaufort Sea. *Arctic*, 41: 48–52.

Holland, P. R., Jenkins, A., and Holland, D. M., 2008: The response of ice shelf basal melting to variations in ocean temperature. *Journal of Climate*, 21: doi:10.1175/2007JCLI1909.1171.

Hoque, M. A., and Pollard, W. H., 2009: Arctic coastal retreat through block failure. *Canadian Geotechnical Journal*, 46: 1103–1115.

Jones, B. M., Hinkel, K. M., Arp, C. D., and Eisner, W. R., 2008: Modern erosion rates and loss of coastal features and sites, Beaufort Sea coastline, Alaska. *Arctic*, 61: 361–372.

Jones, B. M., Arp, C. D., Jorgenson, M. T., Hinkel, K. M., Schmutz, J. A., and Flint, P. L., 2009: Increase in the rate and uniformity of coastline erosion in Arctic Alaska. *Geophysical Research Letters*, 36: doi:10.1029/2008GL036205.

Jorgenson, M. T., and Brown, J., 2005: Classification of the Alaskan Beaufort Sea coast and estimation of carbon and sediment inputs from coastal erosion. *Geo-Marine Letters*, 25: 69–80.

Josberger, E. G., and Martin, S., 1981: A laboratory and theoretical study of the boundary layer adjacent to a vertical melting ice wall in salt water. *Journal of Fluid Mechanics*, 111: 439–473.

Kobayashi, N., 1985: Formation of thermoerosional niches into frozen bluffs due to storm surges on the Beaufort Sea coast. *Journal of Geophysical Research*, 90: 11983–11989.

Kobayashi, N., Vidrine, J. C., Nairn, R. B., and Solomon, S. M., 1999: Erosion of frozen cliffs due to storm surge on Beaufort Sea coast. *Journal of Coastal Research*, 15: 332–344.

Kubat, I., Sayed, M., Savage, S. B., Carrieres, T., and Crocker, G., 2007: An operational iceberg deterioration model. Lisbon,

Portugal: *Proceedings of the Seventh International Offshore and Polar Engineering Conference (ISOPE'07)*, 652–657.
Mars, J. S., and Houseknecht, D. W., 2007: Quantitative remote sensing study indicates doubling of coastal erosion rate in past 50 yr along a segment of the arctic coast of Alaska. *Geology*, 35: 583–586.
Overeem, I., Anderson, R. S., Wobus, C. W., Clow, G. D., Urban, F., and Matell, N., in review: Quantifying the role of climate change on the erosion of a permafrost coastline. *Geophysical Research Letters*.
Rachold, V., Grigoriev, M. N., Aré, F. E., Solomon, S., Reimnitz, E., Kassens, H., and Antonov, M., 2000: Coastal erosion vs. riverine sediment discharge in the Arctic Shelf seas. *International Journal of Earth Sciences*, 89: 450–460.
Reimnitz, E., and Maurer, D. K., 1979: Effects of storm surges on the Beaufort Sea coast, northern Alaska. *Arctic*, 32: 329–344.
Reimnitz, E., Graves, S. M., and Barnes, P. W., 1985: Beaufort Sea coastal erosion, shoreline evolution, and sediment flux. *U.S. Geological Survey Open-file Report 85-380*, 78 pp.
Reimnitz, E., Graves, S. M., and Barnes, P. W., 1988: Beaufort Sea coastal erosion, sediment flux, shoreline evolution and the erosional shelf profile. *U.S. Geological Survey Miscellaneous Investigations Series, I-1182-G*, 22 pp. with map.
Russell-Head, D. D., 1980: The melting of free-drifting icebergs. *Annals of Glaciology*, 1: 119–122.
Serreze, M. C., Holland, M. M., and Stroeve, J., 2007: Perspectives on the Arctic's shrinking sea-ice cover. *Science*, 315: 1533–1536. doi:10.1126/science.1139426.
Solomon, S. M., 2005: Spatial and temporal variability of shoreline change in the Beaufort-Mackenzie region, Northwest Territories, Canada. *Geo-Marine Letters*, 25: 127–137.
U.S. Army Corps of Engineers, 1984. *Shore Protection Manual Volume 1*. 4th ed. Vicksburg, Mississippi: Washington, DC: Department of the Army, Coastal Engineering Research Center, 2 vol., 1088 pp.
Walton, C. C., Pichel, W. G., and Sapper, J. F., 1998: The development and operational application of nonlinear algorithms for the measurement of sea surface temperatures with the NOAA polar-orbiting environmental satellites. *Journal of Geophysical Research*, 103: 27999–28012.
White, F. M., Spaulding, M. L., and Gominho, L., 1980: *Theoretical Estimates of the Various Mechanisms Involved in Iceberg Deterioration in the Open Ocean Environment*. Springfield, Virginia: National Technical Information Service Publication CG-D-62-8081-20571.
Williams, J. R., Yeend, W. F., Carter, L. D., and Hamilton, T. D., 1977: Preliminary surficial deposits map of National Petroleum Reserve–Alaska. *U.S. Geological Survey Open-file Report 77-868*: scale 1:500,000.
Wobus, C. W., Anderson, R. S., Overeem, I., Stanton, T., Clow, G. D., and Urban, F., 2010: The role of summertime storms in thermoabrasion of a permafrost coast. *EOS, Transactions of the American Geophysical Union*, 91(52), Abstract EP23A-0770.

MS accepted April 2011